Defeating Image Obfuscation with Deep Learning

Richard McPherson
The University of Texas at Austin
richard@cs.utexas.edu

Reza Shokri
Cornell Tech
shokri@cornell.edu

Vitaly Shmatikov
Cornell Tech
shmat@cs.cornell.edu

ABSTRACT

We demonstrate that modern image recognition methods based on artificial neural networks can recover hidden information from images protected by various forms of obfuscation. The obfuscation techniques considered in this paper are mosaicing (also known as pixelation), blurring (as used by YouTube), and P3, a recently proposed system for privacy-preserving photo sharing that encrypts the significant JPEG coefficients to make images unrecognizable by humans. We empirically show how to train artificial neural networks to successfully identify faces and recognize objects and handwritten digits even if the images are protected using any of the above obfuscation techniques.

1. INTRODUCTION

As user-contributed photographs and videos proliferate online social networks, video-streaming services, and photo-sharing websites, many of them can be found to leak sensitive information about the users who upload them, as well as bystanders accidentally captured in the frame. In addition to the obvious identifiers such as human faces, privacy can be breached by images of physical objects, typed or handwritten text, license plates, contents of computer screens, etc.

Fully encrypting photos and videos before sharing or uploading them blocks direct information leakage, but also destroys information that is not privacy-breaching. Furthermore, encryption prevents many common forms of processing. For example, encrypted photos cannot be easily compressed for network transmission or cloud storage.

Several privacy protection technologies aim to solve this challenge by obfuscating or partially encrypting the sensitive parts of the image while leaving the rest untouched. A classic example of such a technology is facial blurring. It suppresses recognizable facial features but keeps everything else intact, thus preserving the utility of photographs for purposes such as news reporting. These techniques do not provide well-defined privacy guarantees. Privacy is argued informally, by appealing to the human users' inability to recognize faces and other sensitive objects in the transformed images.

We argue that humans may no longer be the "gold standard" for extracting information from visual data. Recent advances in machine learning based on artificial neural networks have led to dramatic improvements in the state of the art for automated image recognition. Trained machine learning models now outperform humans on tasks such as object recognition [15, 20] and determining the geographic location of an image [49]. In this paper, we investigate what these advances mean for privacy protection technologies that rely on obfuscating or partial encrypting sensitive information in images.

Our contributions. We empirically demonstrate how modern image recognition techniques based on artificial neural networks can be used as an adversarial tool to recover hidden sensitive information from "privacy-protected" images. We focus on three privacy technologies. The first is mosaicing (pixelation), which is a popular way of obfuscating faces and numbers. The second is face blurring, as deployed by YouTube [51]. The third is P3 [39], a recently proposed system for privacy-preserving photo sharing that encrypts the significant coefficients in the JPEG representation of the image. P3 aims to make the image unrecognizable yet preserve its JPEG structure and enable servers to perform certain operations on it (e.g., compress it for storage or transmission).

To illustrate how neural networks defeat these privacy protection technologies, we apply them to four datasets that are often used as benchmarks for face, object, and handwritten-digit recognition. All of these tasks have significant privacy implications. For example, successfully recognizing a face can breach the privacy of the person appearing in a recorded video. Recognizing digits can help infer the contents of written text or license plate numbers.

On the MNIST dataset [27] of black and white handwritten digits, our neural network achieves recognition accuracy of almost 80% when the images are "encrypted" using P3 with threshold level 20 (a value recommended by the designers of P3 as striking a good balance between privacy and utility). When the images are mosaiced with windows of resolution 8×8 or smaller, accuracy exceeds 80%. By contrast, the accuracy of random guessing is only 10%.

On the CIFAR-10 dataset [23] of colored images of vehicles and animals, we achieve accuracy of 75% against P3 with threshold 20, 70% for mosaicing with 4×4 windows, and 50% for mosaicing with 8×8 windows, vs. 10% for random guessing.

On the AT&T [2] dataset of black-and-white faces from 40 individuals, we achieve accuracy of 57% against blurring, 97% against P3 with threshold 20, and over 95% against all examined forms of mosaicing, vs. 2.5% for random guessing.

On the FaceScrub [32] dataset of photos of over 530 celebrities, we achieve accuracy of 57% against mosaicing with 16×16 windows and 40% against P3 with threshold 20, vs. 0.19% for random guessing.

The key reason why our attacks work is that we do *not* need to specify the relevant features in advance. We do not even need to understand what exactly is leaked by a partially encrypted or obfuscated image. Instead, neural networks automatically discover the relevant features and learn to exploit the correlations between hidden and visible information (e.g., significant and "insignificant" coefficients

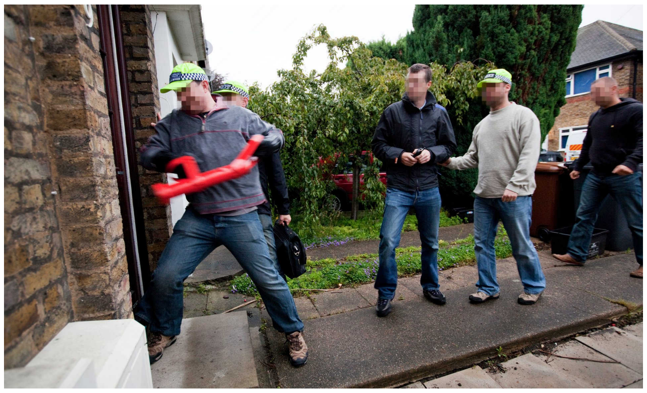

Figure 1: An image from *The Guardian* showing a police raid on a drug gang [28]. The accompanying article explains that UK drug gangs are growing more violent and that police informants and undercover operatives face possible retaliation [1]. The officers' faces are presumably mosaiced for their protection. The window appears to be 12×12 pixels. Using 16×16 windows (which obfuscate more information than 12×12 windows), our neural network achieves 57% accuracy in recognizing an obfuscated image from a large dataset of 530 individuals. The accuracy increases to 72% when considering the top five guesses.

in the JPEG representation of an image). As a consequence, obfuscating an image so as to make it unrecognizable by a human may no longer be sufficient for privacy.

In summary, this paper is the first to demonstrate the power of modern neural networks for adversarial inference, significantly raising the bar for the designers of privacy technologies.

2. IMAGE OBFUSCATION

As the targets for our analysis, we chose three obfuscation techniques that aim to remove sensitive information from images. The first two techniques are *mosaicing* (or pixelation) and *blurring*. These are very popular methods for redacting faces, license plates, adult content, and text (Figure 1). The third technique is a recently proposed system called P3 [39] that aims to protect the privacy of images uploaded to online social networks such as Facebook while still enabling some forms of image processing and compression.

2.1 Mosaicing

Mosaicing (pixelation) is used to obfuscate parts of an image. The section to be obfuscated is divided into a square grid. We refer to the size of each square (a.k.a., "pixel box") as the mosaic window. The average color of every pixel in each square is computed and the entire square is set to that color [16].

The size of the window can be varied to yield more or less privacy. The larger the box, the more pixels will be averaged together and the less fine-grained the resulting mosaiced image will be.

Although the size of the image stays the same, mosaicing can be thought of as reducing the obfuscated section's resolution. For example, a window of size $n \times n$ applied to an image effectively reduces the number of unique pixels in an image by a factor of n^2.

2.2 Blurring

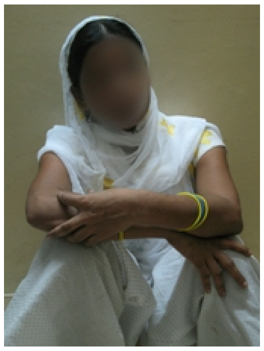

Figure 2: A victim of human trafficking in India [35]. Her face has been blurred, presumably to protect her identity. Our neural networks, trained on black-and-white faces blurred with YouTube, can identify a blurred face with over 50% accuracy from a database of 40 faces.

Blurring (often called "Gaussian blur") is similar to mosaicing and used to obfuscate faces and sensitive text. Blurring removes details from an image by applying a Gaussian kernel [16]. The result is a "smoothed" version of the original image (see Figure 2).

In 2012, YouTube introduced the ability to automatically blur all faces in a video [51]. YouTube presents their automatic facial blurring as a way to improve video privacy. For example, they suggest that it can be used it to "share sensitive protest footage without exposing the faces of the activists involved." In 2016 YouTube introduced the ability to blur arbitrary objects in a video [52]. Once this feature is selected, YouTube will attempt to continue blurring the selected objects as they move around the screen. YouTube claims to have added this feature "with visual anonymity in mind."

Mosaicing and blurring do not remove all information from an image, but aim to prevent human users from recognizing the blurred text or face. The result of these techniques also often used as it is less visually jarring than, for example, a black box produced by full redaction.

In Section 7, we survey prior papers that demonstrated the insufficiency of mosaicing and blurring as a privacy protection technique. To the best of our knowledge, this paper is the first to demonstrate that standard image recognition models can extract information from mosaiced and blurred images.

2.3 P3

Privacy Preserving Photo Sharing (P3) [39] was designed to protect the privacy of JPEG images hosted on social media sites. P3 is intended to be applied by users, but it also assumes that the sites will not prevent users from uploading P3-protected images.

The main idea of P3 is to split each JPEG into a public image and a secret image. The public image contains most of the original image but is intended to exclude the sensitive information. Public images can thus be uploaded to online social networks and untrusted servers. It is essential that the public image is not encrypted and correctly formatted as a JPEG since some popular sites (e.g., Facebook) do not allow users to upload malformed images.

The secret image is much smaller in size but contains most of the sensitive information from the original image. It is

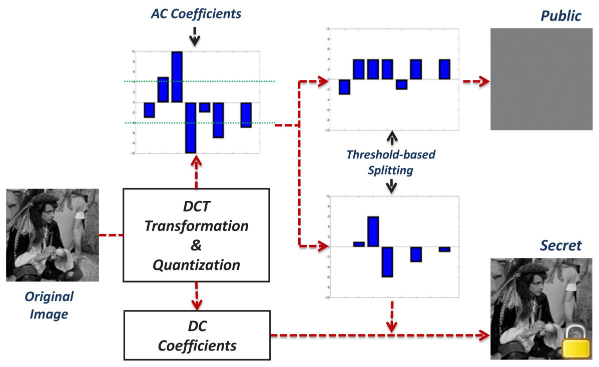

Figure 3: P3 works by removing the DC and large AC coefficients from the public version of image and placing them in a secret image. (Image from [39])

encrypted and uploaded to a third-party hosting service like Dropbox.

Given a public image and a private image, it is easy to combine them back into the original image. P3 proposes a browser plugin that can be used while browsing social media sites. It automatically downloads an encrypted image, decrypts it if the user has the appropriate keys, and displays the combined image. Anyone browsing the social media site without the plugin or the corresponding keys would only see the public parts of images.

P3 supports the recovery of original images even after transformations (e.g., cropping and resizing) are applied to the public image, but the details of this do not affect the privacy properties of P3.

To explain how P3 works, we first review the basics of JPEG image formatting [46]. When converting an image to JPEG, the color values of each block of 8×8 pixels are processed with a discrete cosine transform (DCT), and the resulting DCT coefficients are saved as the image representation (after some additional formatting).

P3 assumes that the DC coefficient (the 0^{th} one) and the larger AC coefficients (the remaining 63) carry the most information about the image. When applying P3 to an image, the user sets a *threshold* value. The DC coefficients, as well as any AC coefficients whose values are larger than the threshold, are encrypted and stored in the secret image (see Figure 3). In the public image, these coefficients are replaced by the threshold value. All remaining AC coefficients are stored in in the public image in plaintext. To reconstruct the original image, the coefficients in the secret image are decrypted and copied to their places in the public image.

By varying the threshold value, the user can balance the size of the secret image against the amount of data removed from the public image. The authors of P3 recommend using threshold values between 10 and 20.

P3 explicitly aims to protect images from "automatic recognition technologies" [39]. P3 uses signal processing tests, including edge detection, face detection, face recognition, and SIFT features, as privacy metrics. Since these features in the public images do not match those in the original images and standard techniques do not find or recognize faces in the public images, the authors of P3 conclude that the system protects privacy. They do not evaluate the human recognition rate of public images, but as examples in Table 1

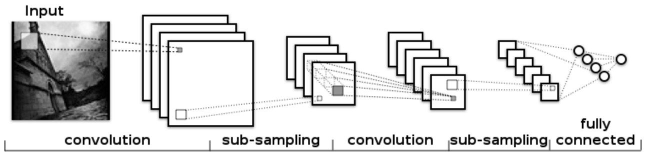

Figure 4: Schematic architecture of a convolutional neural network [9]. The network is composed of convolutional layers followed by max-pooling sub-sampling layers. The last layers are fully connected.

illustrate, public P3 images produced with the recommended threshold values do not appear to be human-recognizable.

3. ARTIFICIAL NEURAL NETWORKS

Neural networks with many layers, also known as deep neural networks, have become very effective in classifying high-dimensional data such as images and speech signals [14, 15, 26]. As opposed to other machine learning algorithms, which require explicit feature specification and engineering, neural networks can, given a classification task, *automatically* extract complex features from high-dimensional data and use these features to find the relationship between the data and the model's output. In this paper, we focus on training neural networks in a supervised setting for classification. The training process involves constructing a model that learns the relationship between data and classes from a labeled dataset (where for each data record we know its true class).

An artificial neural network is composed of multiple layers of nonlinear functions so that more abstract features are computed as nonlinear functions of lower-level features. Each function is modeled as a neuron in the network. The input to the inner layer's neurons is the output of the neurons in the previous layer. The functions implemented in the neurons are referred to as *activation* units and are usually pre-determined by the model designer. The nonlinear functions are constructed to maximize the prediction accuracy of the whole model on a training dataset. In Section 5.4, we give concrete examples of neural networks used for image recognition tasks.

In our networks, we use two activation units: ReLU (rectified linear units) and LeakyReLU. The ReLU is an activation function $f(x) = \max(0, x)$, while the LeakyReLU is the activation function

$$f(x) = \begin{cases} x, & \text{if } x > 1 \\ 0.01x, & \text{otherwise.} \end{cases}$$

Model training or learning is an optimization problem whose objective is to (1) extract the most relevant features for a particular classification task, and (2) find the best relationship between these features and the output of the model (i.e., classification of inputs).

The architecture of the network, which determines how different layers interact with each other, greatly affects the potential accuracy of the model. *Convolutional neural networks* (CNN) are a common deep neural-network architecture for object recognition and image classification, known to yield high prediction accuracy [24, 43]. CNNs have also been widely used for face recognition. Zhou et al. [56] and Parkhi et al. [36] presented CNNs for the Labeled Faces in the Wild database [17] supplemented with large datasets of

Web images. Also, FaceNet [42] is an efficient CNN for facial recognition trained on triplets of two matching and one non-matching facial thumbnails.

As opposed to fully connected neural networks, in which all neurons in one layer are connected to all neurons in the previous layer, in a convolutional neural network each neuron may process the output of only a subset of other neurons. This technique allows the model to embed some known structure of the data (e.g., relationship between neighboring pixels). Figure 4 illustrates the schematic architecture of a convolutional neural network. These networks are composed of multiple convolutional and sub-sampling layers with several fully connected layers at the end. Each neuron in a convolutional layer works on a small connected region of the previous layer (e.g., neighboring pixels in the first layer) over their full depth (e.g., all color signals in the first layer). Usually, multiple convolutional neurons operate on the same region in the previous layer, which results in extracting multiple features for the same region. In the sub-sampling layer, a function of these features is computed and passed to the next layer. Max-pooling, where the feature with the highest value is selected, is typically used for this purpose. After a few convolutional and max-pooling layers, the final layers of the network are fully connected.

Given a network architecture, the training process involves learning the importance weights of each input for each neuron. These weights are referred to as neural-network parameters. The objective is to find the parameter values that minimize the classification error of the model's output. Training is an iterative process. In each iteration (known as a training epoch), the weights are updated so as to reduce the model's error on its training set. This is done by stochastic gradient descent algorithm [40] which computes the gradient of the model's error over each parameter and updates the parameter towards lower errors. The magnitude of the update is controlled by the "learning rate" hyper-parameter.

To avoid overfitting on the training set and to help the trained model generalize to data beyond its training set, various regularization techniques are used. Dropout [45] is an effective regularization technique for neural networks which works by randomly dropping nodes (neurons) during the training with a pre-determined probability.

4. THREAT MODEL

We assume that the adversary has a set of obfuscated images and his goal is to uncover certain types of sensitive information hidden in these images: namely, recognize objects, faces, and/or digits that appear in the image. Recognizing objects or faces from a known set is a standard image recognition task, except that in this case it must be performed on obfuscated images. For example, the operator of a storage service that stores obfuscated photos from an online social network may want to determine which users appear in a given photo.

We also assume that the adversary has access to a set of plain, unobfuscated images that can be used for training the adversary's neural networks. In the case of objects or handwritten digits, the adversary needs many different images of objects and digits. Such datasets are publicly available and used as benchmarks for training image recognition models. In the case of face recognition, the adversary needs the set of possible faces that may appear in a given photo. This is a realistic assumption for online social networks, where the faces of most users are either public, or known to the network operator.

We assume that the adversary knows the exact algorithm used to obfuscate the images but not the cryptographic keys (if any) used during obfuscation. In the case of P3, this means that the adversary knows which threshold level was used but not the keys that encrypt the significant JPEG coefficients. In the case of mosaicing, the adversary knows the size of the pixelation window. In the case of blurring, the adversary has *black-box* access to the blurring algorithm and does not have any information about this algorithm other than what this algorithm produces on adversary-supplied videos and images. This accurately models the case of YouTube blurring, which from the viewpoint of a video creator has a simple on/off switch.

5. METHODOLOGY

5.1 How the attack works

The main idea of our attack is to train artificial neural networks to perform image recognition tasks on obfuscated images. We train a separate neural-network model for each combination of an obfuscation technique and a recognition task.

As explained in Section 4, we assume that the adversary has access to a set of plain, unobfuscated images that he can use for training. We generate the training set by applying the given obfuscation technique to these images (for example, request YouTube's Video Manager to blur the faces). We then perform supervised learning on the obfuscated images to create an obfuscated-image recognition model, as described in Section 5.5. Complete descriptions of our neural-network architectures are in the appendices. Finally, we measure the accuracy of our models.

In all of our experiments, the training set and the test set are disjoint. For example, the images used for training the mosaiced-face recognition model are drawn from the same dataset of facial photos as the images used for measuring the accuracy of this model, but the two subsets have no images in common.

5.2 Datasets

We used four different, diverse datasets: the MNIST database of handwritten digits, the CIFAR-10 image dataset, the AT&T database of faces, and the FaceScrub celebrity facial dataset.

MNIST. The MNIST dataset [27] consists of 28×28 grayscale images of handwritten digits collected from US Census Bureau employees and high-school students. Each image consists of one handwritten digit (i.e., an Arabic numeral between 0 and 9). The dataset is divided into a training set of 60,000 images and a test set of 10,000 images. We expanded the MNIST images to 32x32 images by adding a 2-pixel white border around the edge of each image.

CIFAR-10. The CIFAR-10 dataset [23] consists of 32×32 color images. Each image contains an object belonging to one of 10 classes. Each class is either a vehicle (e.g., plane, car, etc.) or an animal (e.g., dog, cat, etc.). There are 50,000 images in the CIFAR-10 training set and 10,000 images in the test set.

AT&T. The AT&T database of faces [2] contains 400 92×112 grayscale images of 40 individuals. Each individual has 10 images in the dataset, taken under a variety of lighting

		Mosaic				P3		
Dataset	Original	2×2	4×4	8×8	16×16	20	10	1
MNIST	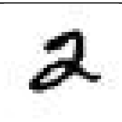	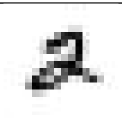	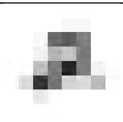	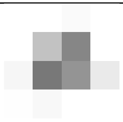	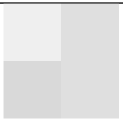	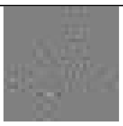	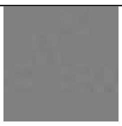	
CIFAR-10	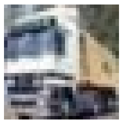	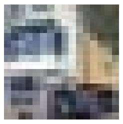	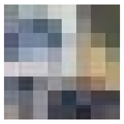	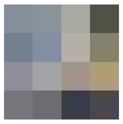	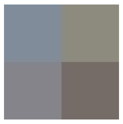		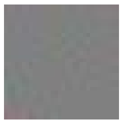	
AT&T	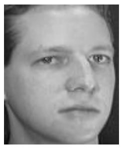	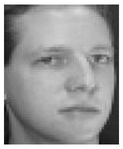	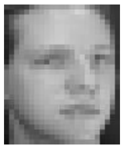	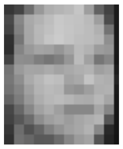	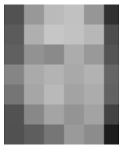			
FaceScrub	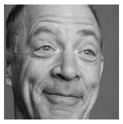	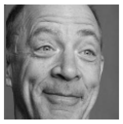	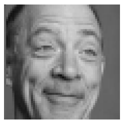	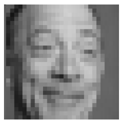	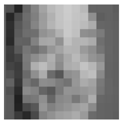	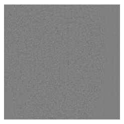	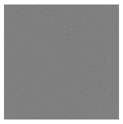	

Table 1: Examples images from each dataset. The leftmost image is the original image. The remaining columns are the image obfuscated with mosaicing with windows of 2×2, 4×4, 8×8, and 16×16 pixels and P3 with thresholds of 20, 10, and 1.

conditions, with different expressions and facial details (i.e., with or without glasses). For our training set, we randomly selected 8 images of each person. The remaining 2 were used in the test set.

FaceScrub. The FaceScrub dataset [32] is a large dataset originally consisting of over 100,000 facial images of 530 celebrities. The images have been compiled from various online articles. Due to copyright concerns only the image URLs are distributed, not the images themselves. Some of the images are no longer accessible and we were able to download only 66,033 images. FaceScrub includes the bounding boxes for the faces in each image and we used those to extract the faces. 10 images of each person was used in the test set, the remaining 60,733 were used for training. Because some of the images are not in color, we converted all images to grayscale and scaled them to 224×224.

5.3 Obfuscation

For mosaicing (pixelation), we used a simple Python script with NumPy [34] to compute the average color of a block of pixels and then change the entire block to that color.

To obfuscate images using the P3 technique, we modified the 9a version of the Independent JPEG Group's JPEG compression software [19] to replace any JPEG coefficient whose absolute value is bigger than the threshold with the threshold value. The resulting image is the same as the public image that would have been produced by P3.

For blurring faces in the AT&T dataset, we used YouTube's facial blurring [51]. For the training and test sets, we used `ffmpeg` to create videos of the original faces from the dataset and uploaded them to YouTube. Each face was shown for 1 second and followed by 1 second of white frames before the next face was shown. Video resolution was 1280×720, with 92×112 faces were centered in their frames.

After uploading the training and test videos, we used YouTube's Video Manager to automatically blur all faces in these videos, then downloaded the videos and used `ffmpeg` to extract each frame. We did not notice any faces that YouTube did not blur, but some edges of a few images were not blurred.

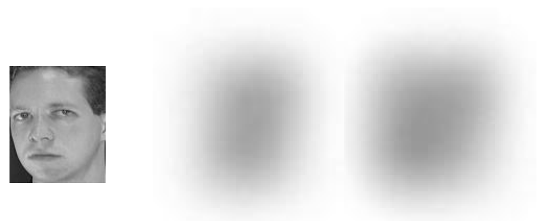
Figure 5: An original AT&T image and two blurred frames extracted from a blurred YouTube video. Although the unblurred frames were identical, the two blurred frames are different.

Although the images in the videos were static, many of the faces in the blurred videos shifted in appearance, that is, parts of an image would become lighter or darker between frames. We do not know if this is a feature added by YouTube to make identification harder or an artifact of their blurring technique. To account for the different blurrings of each image and to avoid any bleeding across images, we used the middle 5 frames of each image in the videos. This increased the size of our training and testing sets to 1,600 and 400 images each.

Because the blurring often extended outside of the original image borders, we extracted the center 184×224 pixels from each frame and then resized them to 92×112 pixels. Two examples of a blurred image can be seen in Figure 5.

5.4 Neural networks

Our experiments were done with three different neural networks: a digit recognition model for the MNIST dataset, an object recognition model for CIFAR-10, and a face recognition model for AT&T and FaceScrub datasets. All of our models are deep convolutional neural networks [21, 24] with dropout [45] regularization.

Note that we use the same architecture for training classification models on the original and obfuscated images. We compare the accuracy of our models on obfuscated images with the accuracy of similar models on the original images. If we had used more accurate neural-network models or tailored neural networks specifically for recognizing obfuscated images, we could have achieved even higher accuracy than reported in this paper.

MNIST. We used a simple neural network for classifying images in the MNIST dataset, based on Torch's template neural network for MNIST [7]. See Appendix A.1 for the exact description of the network architecture.

In this network, each convolutional layer with a leaky rectified linear unit (LeakyReLU) is followed by a layer of pooling. The network ends with a simple fully connected layer and a softmax layer that normalizes the output of the model into classification probabilities. A dropout layer with a probability of 0.5 is introduced between the linear layer and the softmax layer.

CIFAR-10. For CIFAR-10, we used Zagoruyko's CIFAR-10 neural network [54]. This network was created to see how batch normalization worked with dropout. Batch normalization speeds up the training and improves neural networks by normalizing mini-batches between layers inside the neural network [20]. The Zagoruyko method creates a large convolutional neural network and adds batch normalization after every convolutional and linear layer. Zagoruyko's network consists of 13 convolutional layers with batch normalization, each with a rectified linear unit (ReLU). See Appendix A.2 for the exact description of the network architecture.

AT&T and FaceScrub. The networks used for the AT&T and FaceScrub datasets of facial images are similar to the one used on the MNIST dataset, with an extra round of convolution. See Appendix A.3 and A.4 for the exact description of the network architecture.

5.5 Training

For each of our experiments, we obfuscated the entire dataset and then split it into a training set and a test set. In the MNIST and CIFAR-10 datasets, images are already designated as training or test images. For AT&T and FaceScrub, we randomly allocated images to each set.

For training the MNIST model, we used the learning rate of 0.01 with the learning rate decay of 10^{-7}, momentum of 0.9, and weight decay of 5×10^{-4}. The learning rate and momentum control the magnitude of updates to the neural-network parameters during the training [4, 40]. For training the CIFAR-10 model, we initialized the learning rate to 1 and decreased it by a factor of 2 every 25 epochs. Weight decay was 5×10^{-4}, momentum was 0.9, and learning rate decay was 10^{-7}. For the AT&T and FaceScrub models, we used the same learning rate and momentum as in the MNIST training.

We ran all of our experiments for 100-200 training epochs. For each epoch, we trained our neural networks on the obfuscated training set and then measured the accuracy of the network on the obfuscated test set.

Our neural networks were programmed in Torch. The MNIST and AT&T networks were distributed across multiple Linux machines in an HTCondor cluster. The larger CIFAR-10 and FaceScrub networks made use of the Torch CUDA backend and were trained on Amazon AWS g2.8xlarge machines with GRID K520 Nvidia cards running Ubuntu 14.04.

6. RESULTS

From each of the original datasets, we created seven obfuscated datasets for a total of eight datasets (see Table 1). For each neural networks defined in 5.4, we created eight models: one for classifying images in the original dataset and one each for classifying the obfuscated versions of that dataset. In addition to these eight sets, we created a ninth set from the AT&T dataset. This set used facial images that were blurred by YouTube. While the same network was used for all versions of a dataset, the networks were trained and tested on only one version at a time (i.e., there was no mixing between the images obfuscated with different techniques or with the original images).

Three of the obfuscated datasets were created by running P3 on the original images and saving the P3 public images. We used P3 with thresholds of 1, 10, and 20. 10 and 20 are the thresholds recommended by the designers of P3 as striking a good balance between privacy and utility [39]. The threshold of 1 is the most privacy-protective setting that P3 allows.

The remaining four obfuscated datasets were created by mosaicing the original dataset with different windows. Mosaic windows of 2×2, 4×4, 8×8, 16×16 were used. When analyzing the accuracy of our network with different mosaic window sizes, image resolution should be taken into account. For datasets with 32×32 resolution (i.e., MNIST and CIFAR-10), 16×16 windows reduce the practical size of each image to only 2×2 pixels. On the FaceScrub dataset, however, we could maintain the resolution of 14×14 pixels after the image was mosaiced with the same 16×16 window.

We computed the accuracy of the network in classifying the test set after every round of training. We recorded the accuracy of the top guess as well as the top 5 guesses. Results are shown in Table 2.

6.1 MNIST

The results for the MNIST neural network are shown in Figure 6. The accuracy of the neural network on the original images increases quickly and exceeds 90% within 10 epochs. This is not surprising since MNIST is one of the older machine learning datasets and is used pervasively to test models. Top models achieve 98%-99% accuracy [3] and neural networks that can get over 90% accuracy are so simple that they are often used in deep-learning and neural-network tutorials.

The models for mosaiced images with smaller windows (i.e., 2×2 and 4×4) also quickly exceeded 90% accuracy. Although the MNIST images are relatively small, just 32×32 pixels, these small windows have little effect on obscuring the digits. The 2×2 mosaiced images are human-recognizable (see Table 1) and the 4×4 mosaiced images still show the general shape and pixel intensity to a large enough resolution that a neural network can achieve accuracy of over 96%.

The models for the 8×8 and 16×16 mosaiced images reached accuracy of over 80% and 50%, respectively. While these are not as impressive as the other results, it's important to note that mosaicing with these windows reduced the MNIST images to just 4×4 and 2×2 unique pixels. Even the accuracy of 50% is significantly larger than the 10% chance of random guessing the correct digit.

Dataset	Baseline	Original	Mosaic				P3		
			2×2	4×4	8×8	16×16	20	10	1
MNIST Top 1	10.00	98.71	98.49	96.17	83.42	52.13	79.93	74.19	58.54
MNIST Top 5	50.00	100	100	99.95	99.36	93.90	98.91	97.95	94.82
CIFAR Top 1	10.00	89.57	81.76	70.21	53.95	31.81	74.56	65.98	33.21
CIFAR Top 5	50.00	99.46	98.85	97.10	92.26	81.76	96.98	94.99	80.72
AT&T Top 1	2.50	95.00	95.00	96.25	95.00	96.25	97.50	93.75	83.75
AT&T Top 5	12.50	100	100	100	98.75	98.75	100	100	95.00
FaceScrub Top 1	0.19	75.49	71.53	69.91	65.25	57.56	40.02	31.21	17.42
FaceScrub Top 5	0.94	86.06	83.74	82.08	79.13	72.23	58.38	51.28	34.79

Table 2: Accuracy of neural networks classifying the original datasets as well as those obfuscated with mosaicing with windows of 2×2, 4×4, 8×8, and 16×16 pixels and P3 thresholds of 20, 10, and 1. The baseline accuracy corresponds to random guessing.

Dataset	Baseline	Original	Blurred
AT&T Top 1	2.50	95.00	57.75
AT&T Top 5	12.50	100	85.75

Table 3: The accuracy of classifying the **AT&T** faces blurred with YouTube.

The accuracy of recognizing public P3 images falls between the 8×8 and 16×16 mosaicing. The accuracy of the threshold-20 model is just below 80%. Looking at the threshold-20 image, the general shape of the digit can be seen. It is not surprising that the accuracy is close to to the 8×8 mosaicing because P3 follows the JPEG specifications and obfuscates each 8×8 block of pixels separately [46].

6.2 CIFAR-10

The CIFAR-10 model trained on the original images achieved just under 90% accuracy. This is not as high as the MNIST results, but the CIFAR-10 images are much more complex and cluttered than the simple digits from the MNIST dataset. The CIFAR-10 mosaiced results are also not as strong as the MNIST results. While it would seem that the larger amounts of color information would make classification of the original and mosaiced information easier, it also increases the dimensionality and complexity of both the data and the neural network. When using 16×16 windows, the obfuscated CIFAR-10 images are reduced to just four colors. It is impressive that even in this challenging scenario, the accuracy of our neural network is 31%.

The P3 models on threshold-20 and threshold-10 images achieved accuracies of 74% and 66%, respectively. The accuracy on threshold-1 images, however, dropped to only 32%.

6.3 AT&T

The results for the models trained on the AT&T dataset of faces are shown in Figure 8. The models for the original and mosaiced images all achieved over 95% accuracy. For the original images and the smaller mosaicing windows, this is not surprising. The images in the AT&T dataset are 92×112 pixels, much larger than the MNIST and CIFAR-10's resolution of 32×32. Even the 8×8 mosaiced faces are probably recognizable by a human (see Figure 1).

A human might be able to recognize 16×16 mosaiced images as faces, but we hypothesize that individual identification would become challenging at that level of pixelization. However, these mosaiced images have 6×7 resolution and there is still enough information for the neural networks to be able to accurately recognize people in the images.

The models trained on P3 images did not all reach as high an accuracy as the models working against mosaicing, but their accuracy was above 80%, still much higher than the 2.5% accuracy of random guessing. The results for the threshold-20 images are the best, producing correct identification 97% of the time. Looking at the threshold-20 images, rough outlines of faces can be seen, although many of the helpful details, such as differences in color, have been removed by the P3 algorithm. The accuracy of our model was lowest on the threshold-1 images. However, it was still accurate over 83% of the time, which is a major improvement vs. the 2.5% success rate of random guessing.

The AT&T dataset was the only set that we obfuscated with YouTube's facial blurring. Anecdotally, the authors of this paper were at a complete loss when trying to identify the blurred faces by sight. Our simple neural network, however, was able to recognize individuals with 57.75% accuracy (Table 3).

6.4 FaceScrub

The AT&T dataset is relatively small, with only 40 individuals and 10 images per individual. While it is helpful to illustrate the power of neural networks, a larger dataset like FaceScrub, with 530 individuals, is more indicative of achievable accuracy. The full results of the FaceScrub models are shown in Figure 9.

The accuracy of our neural network on the original FaceScrub dataset is 75%. This is impressive for such a simple network on a large dataset. Once again, a more sophisticated network architecture could likely achieve much better results, but our experiments show that even a simple network can defeat the image obfuscation techniques.

The models for recognizing mosaiced faces exhibit the same pattern as the models on the MNIST and CIFAR-10 datasets, with the smaller mosaicing window resulting in the almost the same accuracy as the original images. It is not surprising that the accuracy of recognizing mosaiced faces did not drop below 50%. The FaceScrub images have relatively large resolution, 224×224, thus a 16×16 window only reduces the resolution of the image to 14×14 pixels.

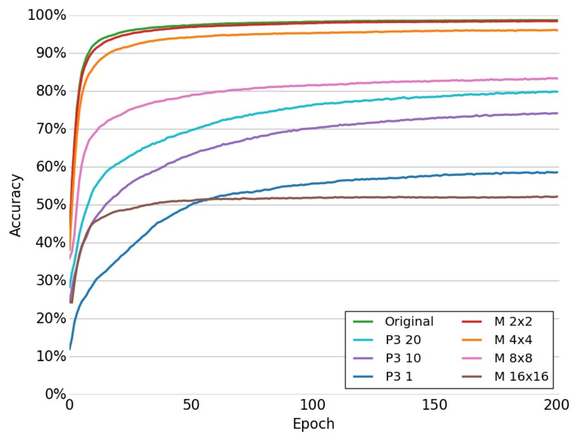

(a) Top guess.

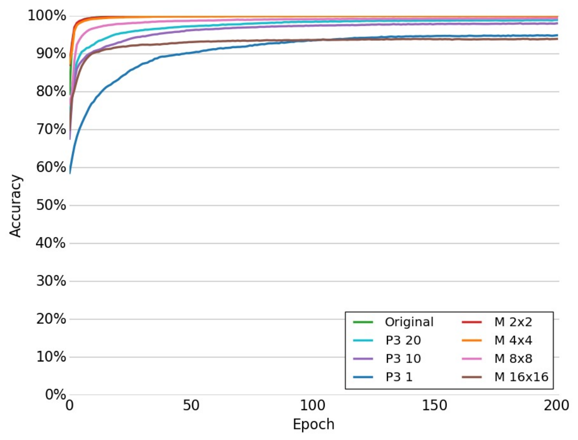

(b) Top 5 guesses.

Figure 6: Test accuracy of the neural networks trained on the **MNIST** handwritten digits. The networks were trained and tested on digits obfuscated with different techniques: P3 with thresholds of 1, 10, and 20, and mosaicing with 2×2, 4×4, 8×8, and 16×16 windows.

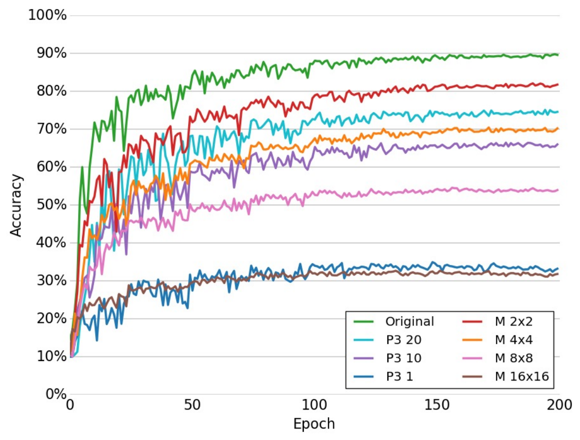

(a) Top guess.

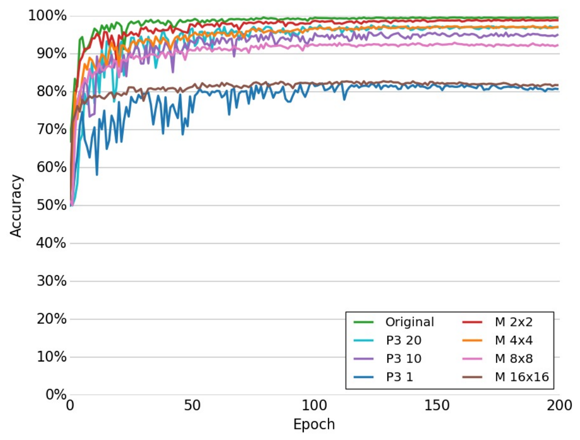

(b) Top 5 guesses.

Figure 7: Test accuracy of the neural networks trained on the **CIFAR-10** images. The networks were trained and tested on colored images obfuscated with different techniques: P3 with thresholds of 1, 10, and 20, and mosaicing with 2×2, 4×4, 8×8, and 16×16 windows.

The results for FaceScrub protected using P3 show some of the worst accuracies in all our experiments. Nevertheless, even the threshold-1 accuracy of 17% is still almost two orders of magnitude larger the accuracy of random guessing (0.19%).

7. RELATED WORK

We survey related work in two areas: image obfuscation and applications of neural networks in security and privacy.

Image obfuscation. Many existing systems and techniques use blurring and mosaicing to protect users' privacy. Face/Off [18] uses facial blurring to prevent identification in "restricted" Facebook images. YouTube supports blurring of faces [51] and objects [52] in videos as well. Google Street View blurs license plates and faces [10].

There is a large body of literature on why simple blurring techniques are insufficient for protecting privacy. To evaluate the effectiveness of blurring and pixelation for hiding identities, Lander et al. [25] asked participants to identify famous people in obfuscated movie clips and static images. Their result show that famous people can still be recognized in some obfuscated images. They also reported higher identification accuracy for movie clips compared to static images. Neustaedter et al. [30] analyzed how obfuscation can balance privacy with awareness in always-on remote video situations, where users would like to recognize the remote person without being able to see the privacy-sensitive parts of the video. Their results show that blurring and pixelation do not achieve both sufficient privacy and satisfactory awareness in remote work settings.

Newton et al. [31] examined many de-identification techniques for obfuscated face images and achieved an extremely high (99%) recognition rate. However, they only considered obfuscating a small rectangle on the top part of the face, including the eyes and top of the nose. Gross et al. [13] designed an algorithmic attack to identify people from their pixelated and blurred face images. Their attack is based on the similarity of the obfuscated image and the original

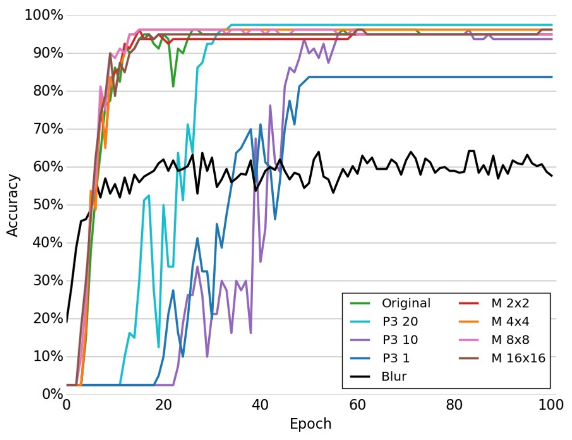

(a) Top guess.

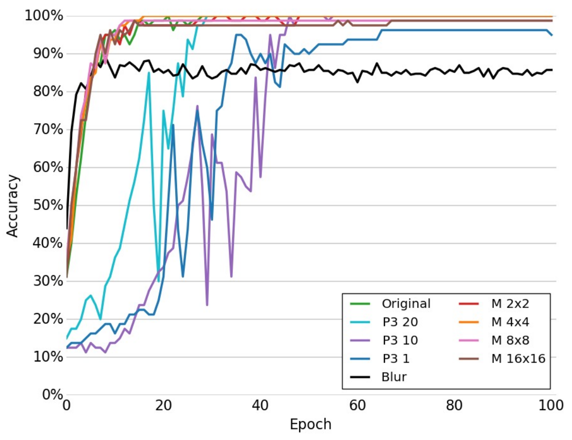

(b) Top 5 guesses.

Figure 8: Test accuracy at each epoch of neural-network training on the **AT&T** dataset of faces. The networks were trained and tested on black-and-white faces obfuscated with different techniques: P3 with thresholds of 1, 10, and 20, mosaicing with 2×2, 4×4, 8×8, and 16×16 windows, and automatic YouTube blurring.

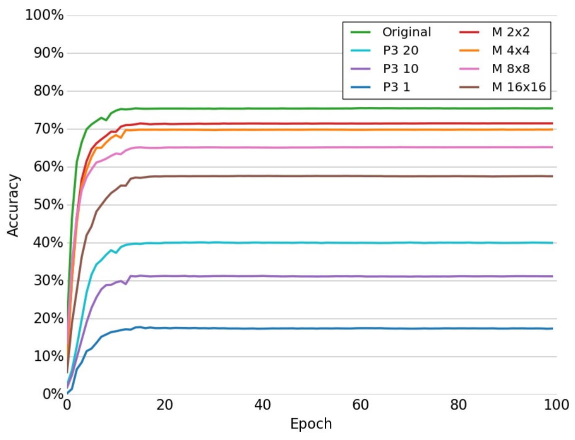

(a) Top guess.

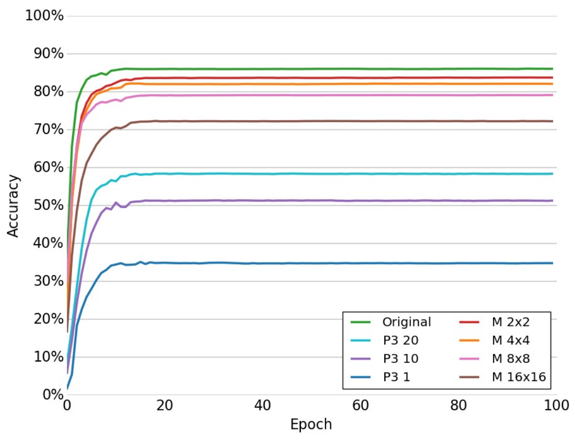

(b) Top 5 guesses.

Figure 9: Test accuracy at each epoch of neural-network training on the **FaceScrub** dataset. The networks were trained and tested on black-and-white celebrity faces obfuscated with different techniques: P3 with thresholds of 1, 10, and 20, mosaicing with 2×2, 4×4, 8×8, and 16×16 windows, and automatic YouTube blurring.

images. They showed that small mosaic boxes (e.g., 2-4 pixels) and simple blurring would not prevent identification attacks. The authors suggested a new de-identification technique based on Newton et al. [31]. Cavedon et al. [6] exploited the changes in pixel boxes for obfuscating video frames to reconstruct pixelated videos using image processing methods so that humans can identify objects in the reconstructed images. Wilber et al. [50] used Facebook's face tagging system as a black-box tool to determine if faces obfuscated with various techniques, including blurring, are still recognizable by Facebook.

Venkatraman [48] presented a brute-force attack to reconstruct pixelated check numbers and concluded that obfuscating sensitive information using blurring provides poor protection, although it might not be easy to reconstruct faces from blurred images. Hill et al. [16] showed that obfuscated text can be reconstructed with a large accuracy using language models. They used hidden Markov models (HMM) to achieve better speed and accuracy vs. Venkatraman's method. They were also able to accurately reconstruct texts when the size of the mosaic box exceeds the size of the letters. Hill's technique relies heavily on knowing the text font and size, as well as the size of the mosaic box.

Gopalan et al. [12] presented a method to recognize faces obfuscated with non-uniform blurring by examining the space spanned by the blurred images. Punnappurath et al. [38] extended this work by applying possible blurring effects to images in the target gallery and finding the minimal distance between the gallery images and the blurred image.

Neural networks. Neural networks have been successfully used extract information from (unobfuscated) images. For example, Golomb et al. [11] used neural networks to identify the sex of human faces.

Beyond their applications in image recognition, (deep) neural networks have been used in many privacy and security contexts. For example, Cannady et al. [5] and Ryan et al. [41] used neural networks in intrusion detection systems

(IDS). Neural networks are particularly useful for this purpose because the IDS designer does not need to engineer relevant network-flow features and can rely on the network to discover these features automatically. Deep neural networks have been used for malware classification in general [8, 37] and for specifically detecting Android malware [53].

Deep convolutional neural networks can be used to detect objects in images. This enables detecting sensitive objects in a video stream or static images. Korayem et al. [22] proposed a technique to detect computer screens in images. The goal is to alert the user or to hide the screen to protect privacy of users who may have sensitive information on their screens. Tran et al. [47] detect privacy-sensitive photos using deep neural networks.

Sivakorn et al. [44] used deep convolutional neural networks to break Google's image CAPTCHAs (which ask users to identify images that have a particular object in them). Melicher et al. [29] used deep neural networks to analyze user passwords and construct a password prediction model.

Concurrently with our work, Oh et al. released a preprint [33] where they use a neural network to recognize untagged individuals in social-media images. Our work differs in several ways: 1) Oh et al. only examine the obfuscation of faces in larger images while we work with entirely obfuscated images (including backgrounds); 2) Oh et al. take advantage of unobfuscated body cues and contextual information in the images to correlate multiple images, whereas we do not make use of any external information beyond the obfuscated image itself; 3) we focus on a broader class of image recognition problems and defeat more types of obfuscation (including, in the case of P3, partially encrypted images that are not recognizable by humans, and real-world protections deployed by popular systems such as YouTube); and 4) Oh et al. only evaluate a single dataset (the People in Photo Albums [55]), whereas we evaluate our attack against diverse datasets, including MNIST, CIFAR-10, AT&T Database of Faces, and FaceScrub. Considering the most comparable results (their unary model of blurred faces across events vs. our blurred faces from the AT&T datasets), our model achieved 18% higher accuracy than theirs.

8. CONCLUSIONS

The experiments in this paper demonstrate a fundamental problem faced by ad hoc image obfuscation techniques. These techniques partially remove sensitive information so as to render certain parts of the image (such as faces and objects) unrecognizable by humans, but retain the image's basic structure and appearance and allow conventional storage, compression, and processing. Unfortunately, we show that obfuscated images contain enough information correlated with the obfuscated content to enable accurate reconstruction of the latter.

Modern image recognition methods based on deep learning are especially powerful in this setting because the adversary does not need to specify the relevant features of obfuscated images in advance or even understand how exactly the remaining information is correlated with the hidden information. We demonstrate that deep learning can be used to accurately recognize faces, objects, and handwritten digits even if the image has been obfuscated by mosaicing, blurring, or encrypting the significant JPEG coefficients.

Instead of informal arguments based on human users' inability to recognize faces and objects in the obfuscated image, the designers of privacy protection technologies for visual data should measure how much information can be reconstructed or inferred from the obfuscated images using state-of-the-art image recognition algorithms. As the power of machine learning grows, this tradeoff will shift in favor of the adversaries. At the other end of the spectrum, full encryption blocks all forms of image recognition, at the cost of destroying all utility of the images.

How to design privacy protection technologies that can, for example, protect faces in photos and videos while preserving the news value of these images is an important topic for future research.

9. REFERENCES

[1] D. Aitkenhead. 'I've done really bad things': The undercover cop who abandoned the war on drugs. *The Guardian*, 2016.

[2] AT&T Laboratories Cambridge. The database of faces, 1994.

[3] R. Benenson. Who is the best at X? http://rodrigob.github.io/are_we_there_yet/build/, 2016.

[4] C. M. Bishop. Pattern recognition. *Machine Learning*, 128, 2006.

[5] J. Cannady. Artificial neural networks for misuse detection. In *National information systems security conference*, 1998.

[6] L. Cavedon, L. Foschini, and G. Vigna. Getting the face behind the squares: Reconstructing pixelized video streams. In *WOOT*, 2011.

[7] R. Collobert, K. Kavukcuoglu, and C. Farabet. Torch7: A matlab-like environment for machine learning. In *BigLearn, NIPS Workshop*, 2011.

[8] G. E. Dahl, J. W. Stokes, L. Deng, and D. Yu. Large-scale malware classification using random projections and neural networks. In *2013 IEEE International Conference on Acoustics, Speech and Signal Processing*, 2013.

[9] Deeplearning.net. Convolutional neural networks (LeNet). http://deeplearning.net/tutorial/lenet.html, 2016.

[10] A. Frome, G. Cheung, A. Abdulkader, M. Zennaro, B. Wu, A. Bissacco, H. Adam, H. Neven, and L. Vincent. Large-scale privacy protection in Google Street View. In *2009 IEEE 12th international conference on computer vision*, 2009.

[11] B. A. Golomb, D. T. Lawrence, and T. J. Sejnowski. SEXNET: A neural network identifies sex from human faces. In *NIPS*, 1990.

[12] R. Gopalan, S. Taheri, P. Turaga, and R. Chellappa. A blur-robust descriptor with applications to face recognition. *IEEE transactions on pattern analysis and machine intelligence*, 2012.

[13] R. Gross, L. Sweeney, F. De la Torre, and S. Baker. Model-based face de-identification. In *CVPRW*, 2006.

[14] A. Hannun, C. Case, J. Casper, B. Catanzaro, G. Diamos, E. Elsen, R. Prenger, S. Satheesh, S. Sengupta, A. Coates, et al. Deep speech: Scaling up end-to-end speech recognition. *arXiv:1412.5567*, 2014.

[15] K. He, X. Zhang, S. Ren, and J. Sun. Delving deep into rectifiers: Surpassing human-level performance on ImageNet classification. In *Proceedings of the IEEE International Conference on Computer Vision*, 2015.

[16] S. Hill, Z. Zhou, L. Saul, and H. Shacham. On the (in) effectiveness of mosaicing and blurring as tools for document redaction. *PETS*, 2016.

[17] G. B. Huang, M. Ramesh, T. Berg, and E. Learned-Miller. Labeled faces in the wild: A database for studying face recognition in unconstrained environments. Technical report, Technical Report 07-49, University of Massachusetts, Amherst, 2007.

[18] P. Ilia, I. Polakis, E. Athanasopoulos, F. Maggi, and S. Ioannidis. Face/off: Preventing privacy leakage from photos in social networks. In *CCS*, 2015.

[19] Independent JPEG Group. Independent JPEG group. http://www.ijg.org/, 2012.

[20] S. Ioffe and C. Szegedy. Batch normalization: Accelerating deep network training by reducing internal covariate shift. *arXiv:1502.03167*, 2015.

[21] K. Jarrett, K. Kavukcuoglu, Y. Lecun, et al. What is the best multi-stage architecture for object recognition? In *2009 IEEE 12th International Conference on Computer Vision*, pages 2146–2153. IEEE, 2009.

[22] M. Korayem, R. Templeman, D. Chen, and D. C. A. Kapadia. Enhancing lifelogging privacy by detecting screens. In *Proceedings of the 2016 CHI Conference on Human Factors in Computing Systems*, 2016.

[23] A. Krizhevsky and G. Hinton. Learning multiple layers of features from tiny images, 2009.

[24] A. Krizhevsky, I. Sutskever, and G. E. Hinton. ImageNet classification with deep convolutional neural networks. In *Advances in neural information processing systems*, 2012.

[25] K. Lander, V. Bruce, and H. Hill. Evaluating the effectiveness of pixelation and blurring on masking the identity of familiar faces. *Applied Cognitive Psychology*, 2001.

[26] Y. LeCun, Y. Bengio, and G. Hinton. Deep learning. *Nature*, 2015.

[27] Y. LeCun, C. Cortes, and C. J. Burges. The mnist database of handwritten digits, 1998.

[28] D. Levene. A police raid in London in 2011. *The Guardian*, 2011.

[29] W. Melicher, B. Ur, S. M. Segreti, S. Komanduri, L. Bauer, N. Christin, and L. F. Cranor. Fast, lean and accurate: Modeling password guessability using neural networks. In *Proceedings of USENIX Security*, 2016.

[30] C. Neustaedter, S. Greenberg, and M. Boyle. Blur filtration fails to preserve privacy for home-based video conferencing. *ACM Transactions on Computer-Human Interaction (TOCHI)*, 2006.

[31] E. M. Newton, L. Sweeney, and B. Malin. Preserving privacy by de-identifying face images. *IEEE transactions on Knowledge and Data Engineering*, 2005.

[32] H.-W. Ng and S. Winkler. A data-driven approach to cleaning large face datasets. In *IEEE International Conference on Image Processing (ICIP)*, 2014.

[33] S. J. Oh, R. Benenson, M. Fritz, and B. Schiele. Faceless person recognition; privacy implications in social media. *arXiv:1607.08438*, 2016.

[34] T. E. Oliphant. Python for scientific computing. *Computing in Science & Engineering*, 2007.

[35] U. N. O. on Drugs and Crime. India: Community vigilance rescues Roshni. 2010.

[36] O. M. Parkhi, A. Vedaldi, and A. Zisserman. Deep face recognition. In *British Machine Vision Conference*, 2015.

[37] R. Pascanu, J. W. Stokes, H. Sanossian, M. Marinescu, and A. Thomas. Malware classification with recurrent networks. In *ICASSP*, 2015.

[38] A. Punnappurath, A. N. Rajagopalan, S. Taheri, R. Chellappa, and G. Seetharaman. Face recognition across non-uniform motion blur, illumination, and pose. *IEEE Transactions on Image Processing*, 2015.

[39] M.-R. Ra, R. Govindan, and A. Ortega. P3: Toward privacy-preserving photo sharing. In *NSDI*, 2013.

[40] D. E. Rumelhart, G. E. Hinton, and R. J. Williams. Learning representations by back-propagating errors. *Cognitive modeling*, 5(3):1, 1988.

[41] J. Ryan, M.-J. Lin, and R. Miikkulainen. Intrusion detection with neural networks. *Advances in neural information processing systems*, 1998.

[42] F. Schroff, D. Kalenichenko, and J. Philbin. Facenet: A unified embedding for face recognition and clustering. In *Proceedings of the IEEE Conference on Computer Vision and Pattern Recognition*, 2015.

[43] K. Simonyan and A. Zisserman. Very deep convolutional networks for large-scale image recognition. *arXiv preprint arXiv:1409.1556*, 2014.

[44] S. Sivakorn, I. Polakis, and A. D. Keromytis. I am robot:(deep) learning to break semantic image captchas. In *2016 IEEE European Symposium on Security and Privacy (EuroS&P)*, 2016.

[45] N. Srivastava, G. E. Hinton, A. Krizhevsky, I. Sutskever, and R. Salakhutdinov. Dropout: a simple way to prevent neural networks from overfitting. *JMLR*, 2014.

[46] Standard, JPEG. Information technology-digital compression and coding of continuous-tone still images-requirements and guidelines. *International Telecommunication Union. CCITT recommendation*, 1992.

[47] L. Tran, D. Kong, H. Jin, and J. Liu. Privacy-cnh: A framework to detect photo privacy with convolutional neural network using hierarchical features. *AAAI 2016*, 2016.

[48] D. Venkatraman. Why blurring sensitive information is a bad idea. https://dheera.net/projects/blur, 2014.

[49] T. Weyand, I. Kostrikov, and J. Philbin. Planet-photo geolocation with convolutional neural networks. *arXiv:1602.05314*, 2016.

[50] M. J. Wilber, V. Shmatikov, and S. Belongie. Can we still avoid automatic face detection? In *WACV*, 2016.

[51] YouTube Official Blog. Face blurring: when footage requires anonymity. https://youtube.googleblog.com/2012/07/face-blurring-when-footage-requires.html, 2012.

[52] YouTube Official Blog. Face blurring: when footage requires anonymity. https://youtube-creators.googleblog.com/2016/02/blur-moving-objects-in-your-video-with.html, 2016.

[53] Z. Yuan, Y. Lu, Z. Wang, and Y. Xue. Droid-sec: Deep learning in Android malware detection. In *ACM SIGCOMM Computer Communication Review*, 2014.

[54] S. Zagoruyko. 92.45% on CIFAR-10 in Torch. http://torch.ch/blog/2015/07/30/cifar.html, 2015.

[55] N. Zhang, M. Paluri, Y. Taigman, R. Fergus, and L. Bourdev. Beyond frontal faces: Improving person recognition using multiple cues. In *CVPR*, 2015.

[56] E. Zhou, Z. Cao, and Q. Yin. Naive-deep face recognition: Touching the limit of LFW benchmark or not? *arXiv:1501.04690*, 2015.

Appendices

A. NEURAL NETWORK ARCHITECTURES

A.1 MNIST Neural Network

```
nn.Sequential {
  [input -> (1) -> (2) -> ... -> (11) -> (12) -> output]
  (1): nn.SpatialConvolutionMM(1 -> 32, 5x5)
  (2): nn.LeakyReLU(0.01)
  (3): nn.SpatialMaxPooling(3x3, 3,3)
  (4): nn.SpatialConvolutionMM(32 -> 64, 5x5)
  (5): nn.LeakyReLU(0.01)
  (6): nn.SpatialMaxPooling(2x2, 2,2)
  (7): nn.Reshape(256)
  (8): nn.Linear(256 -> 200)
  (9): nn.LeakyReLU(0.01)
  (10): nn.Dropout(0.500000)
  (11): nn.Linear(200 -> 10)
  (12): nn.LogSoftMax
}
```

A.2 CIFAR Neural Network

```
nn.Sequential {
 [input -> (1) -> (2) -> (3) -> output]
 (1): nn.BatchFlip
 (2): nn.Copy
 (3): nn.Sequential {
   [input -> (1) -> (2) -> ... -> (53) -> (54) -> output]
   (1): nn.SpatialConvolution(3 -> 64, 3x3, 1,1, 1,1)
   (2): nn.SpatialBatchNormalization
   (3): nn.ReLU
  (4): nn.Dropout(0.300000)
   (5): nn.SpatialConvolution(64 -> 64, 3x3, 1,1, 1,1)
   (6): nn.SpatialBatchNormalization
   (7): nn.ReLU
   (8): nn.SpatialMaxPooling(2x2, 2,2)
   (9): nn.SpatialConvolution(64 -> 128, 3x3, 1,1, 1,1)
   (10): nn.SpatialBatchNormalization
   (11): nn.ReLU
   (12): nn.Dropout(0.400000)
   (13): nn.SpatialConvolution(128 -> 128, 3x3, 1,1, 1,1)
   (14): nn.SpatialBatchNormalization
   (15): nn.ReLU
   (16): nn.SpatialMaxPooling(2x2, 2,2)
   (17): nn.SpatialConvolution(128 -> 256, 3x3, 1,1, 1,1)
   (18): nn.SpatialBatchNormalization
   (19): nn.ReLU
   (20): nn.Dropout(0.400000)
   (21): nn.SpatialConvolution(256 -> 256, 3x3, 1,1, 1,1)
   (22): nn.SpatialBatchNormalization
   (23): nn.ReLU
   (24): nn.Dropout(0.400000)
   (25): nn.SpatialConvolution(256 -> 256, 3x3, 1,1, 1,1)
   (26): nn.SpatialBatchNormalization
   (27): nn.ReLU
   (28): nn.SpatialMaxPooling(2x2, 2,2)
   (29): nn.SpatialConvolution(256 -> 512, 3x3, 1,1, 1,1)
   (30): nn.SpatialBatchNormalization
   (31): nn.ReLU
   (32): nn.Dropout(0.400000)
   (33): nn.SpatialConvolution(512 -> 512, 3x3, 1,1, 1,1)
   (34): nn.SpatialBatchNormalization
   (35): nn.ReLU
   (36): nn.Dropout(0.400000)
   (37): nn.SpatialConvolution(512 -> 512, 3x3, 1,1, 1,1)
   (38): nn.SpatialBatchNormalization
   (39): nn.ReLU
   (40): nn.SpatialMaxPooling(2x2, 2,2)
   (41): nn.SpatialConvolution(512 -> 512, 3x3, 1,1, 1,1)
   (42): nn.SpatialBatchNormalization
   (43): nn.ReLU
   (44): nn.Dropout(0.400000)
   (45): nn.SpatialConvolution(512 -> 512, 3x3, 1,1, 1,1)
   (46): nn.SpatialBatchNormalization
   (47): nn.ReLU
   (48): nn.Dropout(0.400000)
   (49): nn.SpatialConvolution(512 -> 512, 3x3, 1,1, 1,1)
   (50): nn.SpatialBatchNormalization
   (51): nn.ReLU
   (52): nn.SpatialMaxPooling(2x2, 2,2)
   (53): nn.View(512)
   (54): nn.Sequential {
     [input -> (1) -> (2) -> ... -> (5) -> (6) -> output]
     (1): nn.Dropout(0.500000)
     (2): nn.Linear(512 -> 512)
     (3): nn.BatchNormalization
     (4): nn.ReLU
     (5): nn.Dropout(0.500000)
     (6): nn.Linear(512 -> 10)
   }
 }
}
```

A.3 AT&T Neural Network

```
nn.Sequential {
  [input -> (1) -> (2) -> ... -> (14) -> (15) -> output]
  (1): nn.SpatialConvolutionMM(1 -> 32, 3x3, 1,1, 1,1)
  (2): nn.LeakyReLU(0.01)
  (3): nn.SpatialMaxPooling(2x2, 2,2)
  (4): nn.SpatialConvolutionMM(32 -> 64, 3x3, 1,1, 1,1)
  (5): nn.LeakyReLU(0.01)
  (6): nn.SpatialMaxPooling(2x2, 2,2)
  (7): nn.SpatialConvolutionMM(64 -> 128, 3x3, 1,1, 1,1)
  (8): nn.LeakyReLU(0.01)
  (9): nn.SpatialMaxPooling(3x3, 3,3)
  (10): nn.Reshape(8064)
  (11): nn.Linear(8064 -> 1024)
  (12): nn.LeakyReLU(0.01)
  (13): nn.Dropout(0.500000)
  (14): nn.Linear(1024 -> 40)
  (15): nn.LogSoftMax
}
```

A.4 FaceScrub Neural Network

```
FaceScrub
nn.Sequential {
  [input -> (1) -> (2) -> ... -> (13) -> (14) -> output]
  (1): nn.SpatialConvolutionMM(1 -> 32, 3x3, 1,1, 1,1)
  (2): nn.LeakyReLU(0.01)
  (3): nn.SpatialMaxPooling(2x2, 2,2)
  (4): nn.SpatialConvolutionMM(32 -> 64, 3x3, 1,1, 1,1)
  (5): nn.LeakyReLU(0.01)
  (6): nn.SpatialMaxPooling(2x2, 2,2)
  (7): nn.SpatialConvolutionMM(64 -> 128, 3x3, 1,1, 1,1)
  (8): nn.LeakyReLU(0.01)
  (9): nn.SpatialMaxPooling(2x2, 2,2)
  (10): nn.Reshape(100352)
  (11): nn.Linear(100352 -> 1024)
  (12): nn.LeakyReLU(0.01)
  (13): nn.Dropout(0.500000)
  (14): nn.Linear(1024 -> 530)
}
```